Passive cyclotron current generation with fish-scale structures

W. Kernbichler[a)]
Institut für Theoretische Physik, Technische Universität Graz, Petersgasse 16, A-8010 Graz, Austria

S. V. Kasilov
Institute of Plasma Physics, National Science Center, Kharkov Institute of Physics and Technology, Akademicheskaya 1, 310108 Kharkov, Ukraine

(Received 31 May 1996; accepted 14 August 1996)

The paper presents a theoretical and a numerical treatment of the problem of passive current drive in a fusion plasma. In such a scenario the current is driven by the self-generated cyclotron radiation. The necessary asymmetry is introduced with the help of fish-scale structures on the reflecting wall which surrounds the plasma. The problem of the photon equilibrium in a bounded system is the subject of the first part of this paper. The general case of a plasma surrounded by a reflecting wall is presented in the form of a Fredholm integral equation of the second kind. This integral equation is then simplified for small fish-scale-like structures on the first wall with the help of a probabilistic approach. A self-consistent solution for the radiation intensity distribution is obtained numerically for a cylindrical plasma model under such boundary conditions. Based on this and on local current drive efficiencies derived in a companion paper [S. V. Kasilov and W. Kernbichler, Phys. Plasmas, **3**, 4115 (1996)], the radial profile of a steady toroidal current as well as overall efficiencies are computed. © *1996 American Institute of Physics.* [S1070-664X(96)04411-4]

I. INTRODUCTION

The problem of stationary current sustainment in a tokamak device is one of the most important problems in fusion research. In order to drive a toroidal current within a plasma, one has the possibility either to use external sources, as in electron cyclotron resonance heating and current drive (ECRH), ion cyclotron resonance heating and current drive (ICRH), lower hybrid current drive (LH), and neutral beam current drive (NB), or internal sources, as in the case of the bootstrap current.

External methods for current drive have some disadvantages in that it is always necessary to convert fusion power output to electricity and back to current drive power. Every such conversion process is inevitably associated with some efficiency, which in some cases might not be close to unity. In addition to this, the external methods with poor current drive efficiency I/P result in a big amount of circulating power. But in turn, with external systems, one has very good control possibilities through the regulation of the external devices.

Internal current drive systems do not rely on any external power conversion, so there is no external efficiency involved and therefore no external losses to be considered and no external devices to be built. But this advantage is somewhat impaired by the lack of an external control mechanism.

The bootstrap current depends mainly on profiles of density and temperature and the poloidal magnetic field. However, a tokamak equilibrium sustained just with bootstrap current needs a seed current in the plasma center or relies on very strong transport in the plasma core. Advanced tokamak theory tries to find good solutions to this problem and tries to optimize bootstrap current profiles.

A very interesting, and up to now, unique solution to the above-mentioned problems is the so-called passive cyclotron current drive method proposed by Dawson and Kaw.[1] It unifies the advantage of being an internal method with the high enough efficiency pertinent to methods which use the electrons in the tail of the Maxwellian distribution.[2,3] The method relies on asymmetries in the radiation intensity introduced to the system through asymmetries of the wall (e.g., small fish-scale-like structures).

This method could provide a solution for a bootstrap-current-sustained tokamak equilibrium, at least for high-field and high-temperature plasmas, because in most cases it gives a peaked current profile with strong current in the center, as is shown in particular in the present paper. Of course, this type of current drive does not come for free, because with the use of such structures, the loss from the plasma will be inevitably increased, as was originally foreseen.

Up to now, this passive cyclotron current drive method was studied mainly in terms of efficiency.[4–7] However, the problem was not solved in a self-consistent way, which has to take into account the wall structure effects on the radiation intensity distribution in the plasma. Such an approach naturally results in current density profiles which up to now were only obtained through the application of scaling laws.[5]

The present paper is devoted to such a self-consistent study. Here the main focus is on the problem of photon distribution (or in other words radiation intensity distribution) within the plasma and on the resulting profiles for the energy loss and for the steady toroidal current. This problem was actually decoupled from the linked set of nonlinear equations describing the balance between electrons and photons in mildly relativistic, strongly magnetized plasmas in Refs. 8 and 9. The decoupling and linearization of the kinetic equation for the electrons and the equation of radiation transfer becomes a nontrivial problem for plasmas with strong circulation of ''thermal'' cyclotron radiation. This is pertinent to high-temperature, high-field plasmas with low values of

a)Electronic-mail: kernbichler@itp.tu-graz.ac.at

 1070-664X/96/3(11)/4128/12/$10.00

$\beta_e < 0.1$. Such a plasma could be used for advanced reactors.

The resulting linearized kinetic equation for electrons was resolved in Ref. 9 in terms of a passive cyclotron current drive efficiency. This efficiency, in turn, is used in the present paper together with the radiation intensity distribution for the computation of a steady toroidal current.

The structure of the paper is the following: In Sec. II the equation for the transfer of radiation intensity and the expressions for power loss and steady current density are introduced. In Sec. III the formal solution of the linearized problem of radiation transfer in a bounded system (plasma surrounded by some wall) is developed in a general case. As a result, an integral equation for the intensity is obtained. In Sec. IV this equation is simplified for the case of a cylindrical plasma with small fish-scale structures on the reflecting wall. This simplification is done with a probabilistic approach. Within this approach, this integral equation is reduced to a one-dimensional Fredholm type integral equation of the second kind.

A reference parameter set for the numerical study of cyclotron losses and passive cyclotron current drive is introduced in Sec. V. The results of the numerical computation are presented and discussed in Sec. VI. In particular, the radial profiles of power loss and steady toroidal current are shown for the cases of both zero and finite toroidicity. Since a straight-cylinder model is used in the computation, only the effect of toroidicity on the kinetics of electrons (trapped particles, reduction of background response) is included. The effects of a variation of the parameters governing the plasma and the fish-scale properties are also studied in Sec. VI. Approximate scaling expressions for the passively driven current and optimal parameters of the fish-scale structure are discussed there.

II. TRANSFER OF RADIATION, POWER LOSS, AND CURRENT DENSITY

The purpose here is to obtain the radiation intensity distribution $I = I_\omega^{(M)}(\mathbf{r},\mathbf{\Omega})$ in the plasma with the assumption that the electron distribution function is Maxwellian

$$f_0 = \frac{n_e \mu}{4\pi m^3 c^3 K_2(\mu)} \exp(-\mu\gamma). \tag{1}$$

Here $\mathbf{r}$ denotes the position in the plasma, $\mathbf{\Omega} = (\theta,\phi)$ is the solid angle of wave propagation, with θ being the wave pitch angle between the wave vector $\mathbf{k}$ and the magnetic field, and ϕ being an azimuthal angle. The index $M = O,X$ denotes the ordinary and the extraordinary mode of propagation and ω is the radiation frequency. In Eq. (1), K_2 is the modified Bessel function, $\mu = mc^2/T$ is the inverse temperature, and $\gamma = \sqrt{1+u^2}$ is the relativistic factor, with $\mathbf{u} = \mathbf{p}/(mc)$ being the dimensionless electron momentum.

The validity conditions for this assumption in high-temperature fusion plasmas with strong influence of cyclotron radiation on the electron distribution have been discussed in Ref. 9.

Another assumption used in this paper is the absence of refraction for cyclotron radiation. This is common for literature on cyclotron losses[10,11] because the ray refractive index—n_r—is close to unity for all frequencies being of interest for cyclotron power loss. This assumption implies that all rays through the plasma propagate on straight lines. With these two assumptions the equation of transfer of radiation for the intensity I can be written as

$$\mathrm{div}(\hat{\mathbf{k}} I_\omega^{(M)}(\mathbf{r},\mathbf{\Omega})) = j_\omega^{(M)}(\mathbf{r},\mathbf{\Omega}) - \alpha_\omega^{(M)}(\mathbf{r},\mathbf{\Omega}) I_\omega^{(M)}(\mathbf{r},\mathbf{\Omega}). \tag{2}$$

The quantities α_ω and j_ω are the unperturbed absorption and emission coefficients

$$\begin{Bmatrix} \alpha_\omega^{(M)}(\mathbf{\Omega}) \\ j_\omega^{(M)}(\mathbf{\Omega}) \end{Bmatrix} = \frac{4\pi^2 e^2}{mc} \int dP \, \frac{\gamma}{\omega} D_n^{(M)} \times \delta\left(\gamma - \frac{n\omega_{ce}}{\omega} - u_\parallel \cos\theta\right) \begin{Bmatrix} -\hat{L}_n \\ I_{\mathrm{RJ}}\mu \end{Bmatrix} f_0, \tag{3}$$

where ω_{ce} is the cyclotron frequency for a particle at rest. Throughout the paper the dimensionless frequency $\overline{\omega} = \omega/\omega_{ce}$ is also used. The following short notation for electron and photon phase space integration is used:

$$\int dP \equiv \sum_{n=-\infty}^{\infty} \int d^3p = 2\pi m^3 c^3 \sum_{n=-\infty}^{\infty} \int_{-\infty}^{\infty} du_\parallel \int_0^{\infty} du_\perp \, u_\perp, \tag{4}$$

$$\int dK \equiv \sum_{M=O,X} \int_0^{\infty} d\omega \int_{4\pi} d^2\Omega = \sum_{M=o,x} \int_0^{\infty} d\omega \int_{-\pi}^{\pi} d\phi \int_0^{\pi} d\theta \sin\theta, \tag{5}$$

with $u_\parallel$ and $u_\perp$ being the transverse and parallel components of $\mathbf{u}$. The blackbody radiation intensity in the Rayleigh–Jeans limit is defined as

$$I_{\mathrm{RJ}} = \omega^2 T/(8\pi^3 c^2), \tag{6}$$

where the polarization factors are given as

$$D_n^{(X)} = \left(\frac{u_\perp}{\gamma} J_n'(\lambda)\right)^2, \quad D_n^{(O)} = \left(\frac{\gamma\cos\theta - u_\parallel}{\gamma \sin\theta} J_n(\lambda)\right)^2, \tag{7}$$

with J and J' denoting the Bessel function and its derivative, respectively, with its argument λ being

$$\lambda = \frac{n u_\perp \sin\theta}{\gamma - u_\parallel \cos\theta}. \tag{8}$$

The operator $\hat{L}_n$ is defined as

$$\hat{L}_n = \frac{n\omega_{ce}}{\omega u_\perp} \frac{\partial}{\partial u_\perp} + \cos\theta \frac{\partial}{\partial u_\parallel}. \tag{9}$$

The volume density of the power loss determined by the local balance between absorption and emission can be written as

$$p(\mathbf{r})=\sum_{M=O,X} p^{(M)}(\mathbf{r})=\int dK[j_\omega^{(M)}(\mathbf{r},\mathbf{\Omega}) - \alpha_\omega^{(M)}(\mathbf{r},\mathbf{\Omega})I_\omega^{(M)}(\mathbf{r},\mathbf{\Omega})] = \int dK\ \alpha_\omega^{(M)}(\mathbf{r},\mathbf{\Omega})[I_{\mathrm{RJ}}(\mathbf{r}) - I_\omega^{(M)}(\mathbf{r},\mathbf{\Omega})]. \tag{10}$$

In analogy to Eq. (10), where the absorption coefficient links the intensity to the power loss per unit volume, the passively driven current can be expressed as

$$j_\parallel=\int dK\ \eta_\omega^{(M)}(\theta)I_\omega^{(M)}(\theta,\phi), \tag{11}$$

where $\eta_\omega^{(M)}$ is the current drive efficiency derived in Ref. 9. This equation holds as long as there is no poloidal variation of the quantities $\eta_\omega^{(M)}$ and $I_\omega^{(M)}$. Obviously this is the case for straight cylinder geometry.

In the case of toroidal geometry, Eq. (11) has to be modified to

$$j_t=\left\langle \int dK\ \eta_\omega^{(M)}(\theta,\vartheta)I_\omega^{(M)}(\theta,\Phi,\vartheta)\right\rangle, \tag{12}$$

where ϑ is the poloidal angle. Here the brackets denote the average over the layer between two neighboring magnetic surfaces,[9] also referred to as the poloidal average.

For the straight-cylinder model of a tokamak, which is used in this paper, the radiation intensity $I_\omega^{(M)}$ (being the source for current drive) is independent of the poloidal angle ϑ. Therefore, Eq. (12) can be simplified to

$$j_t=\int dK\langle \eta_\omega^{(M)}\rangle_{\mathrm{cyl}}(\theta)I_\omega^{(M)}(\theta,\Phi), \tag{13}$$

where again $\langle \eta_\omega^{(M)}\rangle_{\mathrm{cyl}}$ is specified in Ref. 9. In such a case, only the effect of toroidicity on the kinetics of electrons (trapped particles, reduction of background response) is included.

III. BOUNDARY PROBLEM

The problem of finding the intensity $I_\omega^{(M)}$ can be reduced to an integral problem for the incoming intensity $I_{\mathrm{inc}} = I_{\mathrm{inc},\omega}^{(M)}(\mathbf{y}_w)$. The term ''incoming'' means that the intensity is taken at the point where the ray hits the surrounding wall. Here the argument $\mathbf{y}_w=(\mathbf{\Omega}_w,\mathbf{r}_w)$ consists of coordinates of the end position of the ray on the reflecting surface $\mathbf{r}_w=(\vartheta_w,\zeta_w)$ and the angles of the ray direction in the spherical coordinate system $\mathbf{\Omega}_w=(\Theta_w,\Phi_w)$. The polar angle Θ_w is counted from some axis staying in the plane of the wall and the azimuthal angle Φ_w is counted from the normal to the wall at the point $\mathbf{r}_w$. For the cylindrical model of a tokamak plasma with straight magnetic field lines, the most convenient choice of the polar axis is the direction of the magnetic field. The angles of propagation associated with the magnetic field $\mathbf{\Omega}$ and the position $\mathbf{r}$ elsewhere on the ray can be formally expressed through the ray trajectories as

$$\mathbf{\Omega}=\mathbf{\Omega}'(\mathbf{y}_w,s),\quad \mathbf{r}=\mathbf{r}'(\mathbf{y}_w,s), \tag{14}$$

where s is the distance between the end point of the ray on the surface and the observation point in the plasma. The set of functions $\mathbf{\Omega}'$ and $\mathbf{r}'$ is determined in the straight ray approximation by the geometry of the reflecting wall and of the magnetic field. From the solution for the equation of radiation transfer (2) the intensity I is expressed through I_{inc} as

$$I_\omega^{(M)}(\mathbf{r},\mathbf{\Omega})=[I_{\mathrm{inc},\omega}^{(M)}(\mathbf{y}_w)-I_{\mathrm{gen},\omega}^{(M)}(\mathbf{y}_w,s)]/d_\omega^{(M)}(\mathbf{y}_w,s). \tag{15}$$

Here the ray attenuation factor $d_\omega^{(M)}$ and the additionally generated intensity $I_{\mathrm{gen},\omega}^{(M)}$ produced in the plasma during ray propagation from the observation point to the wall are given as

$$d_\omega^{(M)}(\mathbf{y}_w,s)=\exp\left\{-\int_0^s ds'\,\alpha_\omega^{(M)}(\mathbf{r}'(\mathbf{y}_w,s'),\mathbf{\Omega}'(\mathbf{y}_w,s'))\right\}, \tag{16}$$

$$I_{\mathrm{gen},\omega}^{(M)}(\mathbf{y}_w,s)=\int_0^s ds'\ j_\omega^{(M)}(\mathbf{r}'(\mathbf{y}_w,s'),\mathbf{\Omega}'(\mathbf{y}_w,s')) \times d_\omega^{(M)}(\mathbf{y}_w,s'), \tag{17}$$

where the integration is always done between the end point of the ray at the wall (0) and the observation point (s). The formal solution of the equation of transfer can be written in the form of a Fredholm integral equation of the second kind for the incoming intensity $\mathbf{I}_{\mathrm{inc}}$

$$\mathbf{I}_{\mathrm{inc}}(\mathbf{y}_w)=\int d^4y'_w\ \overleftrightarrow{\mathbf{K}}(\mathbf{y}_w,\mathbf{y}'_w)\mathbf{I}_{\mathrm{inc}}(\mathbf{y}'_w)+\mathbf{I}_{\mathrm{gen}}(\mathbf{y}_w), \tag{18}$$

where the integration over the variable $\mathbf{y}'_w$ means the subsequent integrations

$$\int_{2\pi} d^2\Omega'_w=\int_0^\pi d\Theta'_w\int_{-\pi/2}^{\pi/2} d\Phi'_w J_{\Omega'_w},$$
$$\oint_S d^2S'=\int_0^{2\pi} d\vartheta'_w\int_0^{2\pi} d\zeta'_w J_{S'}, \tag{19}$$

where $J_{\Omega'_w}=\cos\Phi'_w\sin^2\Theta'_w$ and $J_{S'}d\vartheta'_w d\zeta'_w$ is the element of wall area. Here for simplicity a vector notation was chosen for the intensities

$$\mathbf{I}_{\mathrm{inc}}(\mathbf{y}_w)=\begin{pmatrix} I_{\mathrm{inc},\omega}^{(O)}(\mathbf{y}_w)\\ I_{\mathrm{inc},\omega}^{(X)}(\mathbf{y}_w)\end{pmatrix},\quad \mathbf{I}_{\mathrm{gen}}(\mathbf{y}_w)=\begin{pmatrix} I_{\mathrm{gen},\omega}^{(O)}(\mathbf{y}_w,l(\mathbf{y}_w))\\ I_{\mathrm{gen},\omega}^{(X)}(\mathbf{y}_w,l(\mathbf{y}_w))\end{pmatrix} \tag{20}$$

and $\overleftrightarrow{\mathbf{K}}$ is the tensor kernel of the transformation. The length $l(\mathbf{y}_w)$ is the distance between the end point of the ray and its starting point at another location on the surface. Equation (18) can also be written in a more convenient operator notation

$$\mathbf{I}_{\mathrm{inc}}=\hat{\mathbf{K}}\cdot\mathbf{I}_{\mathrm{inc}}+\mathbf{I}_{\mathrm{gen}}, \tag{21}$$

where the transformation operator $\hat{\mathbf{K}}$ actually is built from two operators,

$$\hat{\mathbf{K}}=\hat{\mathbf{P}}\cdot\hat{\mathbf{R}}. \tag{22}$$

The first one is the propagation operator $\hat{\mathbf{P}}$, expressing the intensity $\mathbf{I}_{\rm inc}(\mathbf{y}_w)$ at the end of the ray (point of interest at the wall) through the initial value on this ray $\mathbf{I}_{\rm ref}(\mathbf{y}'_w)$,

$$\hat{\mathbf{P}}\cdot\mathbf{I}_{\rm ref}=\int d^4y'_w\overleftrightarrow{\mathbf{P}}(\mathbf{y}_w,\mathbf{y}'_w)\mathbf{I}_{\rm ref}(\mathbf{y}'_w)=\mathbf{I}_{\rm inc}(\mathbf{y}_w). \tag{23}$$

The second operator is the reflection operator $\hat{\mathbf{R}}$, expressing the reflected intensity $\mathbf{I}_{\rm ref}(\mathbf{y}_w)$ [which in turn is the initial intensity in Eq. (23)] through the incoming intensity $\mathbf{I}_{\rm inc}(\mathbf{y}'_w)$,

$$\hat{\mathbf{R}}\cdot\mathbf{I}_{\rm inc}=\int d^2\Omega'_w\overleftrightarrow{\mathbf{R}}(\mathbf{\Omega}_w,\mathbf{\Omega}'_w)\mathbf{I}_{\rm inc}(\mathbf{y}'_w)=\mathbf{I}_{\rm ref}(\mathbf{y}_w), \tag{24}$$

where $\overleftrightarrow{\mathbf{R}}$ is only a function of $\mathbf{\Omega}_w$ and $\mathbf{\Omega}'_w$ and has just a parametric dependence on $\mathbf{r}_w$ since reflection is a local process. Therefore integration in Eq. (24) is only performed over $\mathbf{\Omega}'_w$.

The propagation operator in general can be written in the form

$$\hat{\mathbf{P}}\cdot\mathbf{I}_{\rm ref}=\int d^2S'\int d^2\Omega'_w\ \delta[\mathbf{\Omega}_w-\mathbf{O}_P(\mathbf{\Omega}'_w,\mathbf{r}'_w)]\times\delta[\mathbf{r}_w-\mathbf{S}_P(\mathbf{\Omega}'_w,\mathbf{r}'_w)]\overleftrightarrow{\mathbf{D}}(\mathbf{\Omega}_w,\mathbf{r}_w)\mathbf{I}_{\rm ref}(\mathbf{\Omega}'_w,\mathbf{r}'_w). \tag{25}$$

Here $\mathbf{S}_P(\mathbf{\Omega}'_w,\mathbf{r}'_w)$ is the end point of the ray which starts from the point $\mathbf{r}'_w=(\vartheta'_w,\zeta'_w)$ in direction $\mathbf{\Omega}'_w$ and $\mathbf{O}_P(\mathbf{\Omega}'_w,\mathbf{r}'_w)$ means the direction of the ray in its end point expressed through the local angular coordinate system in this end point. The normalization of the δ-functions is the following:

$$\int d^2S\ \delta[\mathbf{r}_w-\mathbf{S}_P(\mathbf{\Omega}'_w,\mathbf{r}'_w)]=1, \tag{26}$$

$$\int d^2\Omega_w\ \delta[\mathbf{\Omega}_w-\mathbf{O}_P(\mathbf{\Omega}'_w,\mathbf{r}'_w)]=1. \tag{27}$$

The tensor $\overleftrightarrow{\mathbf{D}}$ is defined as

$$\overleftrightarrow{\mathbf{D}}(\mathbf{y}_w)=\begin{pmatrix} d_\omega^{(O)}[\mathbf{y}_w,l(\mathbf{y}_w)] & 0\\ 0 & d_\omega^{(X)}[\mathbf{y}_w,l(\mathbf{y}_w)]\end{pmatrix} \tag{28}$$

as long as there is no mode conversion during propagation. Combining Eqs. (24) and (25), performing the $\mathbf{\Omega}'_w$-integration in the propagation operator and then exchanging the variables $\mathbf{\Omega}'_w$ and $\mathbf{\Omega}''_w$, one gets

$$\hat{\mathbf{K}}\cdot\mathbf{I}_{\rm inc}=\int d^2S'\int d^2\Omega'_w\,\frac{J_{\mathbf{\Omega}''_w}}{J_{\mathbf{\Omega}_w}}\frac{1}{J_{\rm can}}\,\delta[\mathbf{r}_w-\mathbf{S}_P(\mathbf{\Omega}''_w,\mathbf{r}'_w)]\times\overleftrightarrow{\mathbf{D}}(\mathbf{\Omega}_w,\mathbf{r}_w)\overleftrightarrow{\mathbf{R}}(\mathbf{\Omega}''_w,\mathbf{\Omega}'_w)\mathbf{I}_{\rm inc}(\mathbf{\Omega}'_w,\mathbf{r}'_w), \tag{29}$$

where $\mathbf{\Omega}''_w$ is a solution to the equation

$$\mathbf{\Omega}_w=\mathbf{O}_P(\mathbf{\Omega}''_w,\mathbf{r}'_w), \tag{30}$$

which expresses the ray angle in the initial point through the ray angle in the end point. Here

$$J_{\rm can}=\left|\frac{\partial[\mathbf{O}_P(\mathbf{\Omega}''_w)]}{\partial(\mathbf{\Omega}''_w)}\right|, \tag{31}$$

where the second argument is omitted as a dummy one.

This completely defines $\overleftrightarrow{\mathbf{K}}$ in Eq. (18); one only has to provide the information on the wall reflectivity.

The reflection tensor $\overleftrightarrow{\mathbf{R}}$ is mainly determined by the wall material and by surface structures. It can have both mirror-like and diffusive reflection properties, so in a general way it can be written as

$$\overleftrightarrow{\mathbf{R}}(\mathbf{\Omega}_w,\mathbf{\Omega}'_w)=(1-\alpha_D)\,\delta[\mathbf{\Omega}_w-\mathbf{O}_R(\mathbf{\Omega}'_w)]\overleftrightarrow{\mathbf{M}}(\mathbf{\Omega}'_w)+\alpha_D\overleftrightarrow{\mathbf{D}}(\mathbf{\Omega}_w,\mathbf{\Omega}'_w). \tag{32}$$

The $\overleftrightarrow{\mathbf{M}}$ and $\overleftrightarrow{\mathbf{D}}$ describe the mirror-like reflection and the diffusive reflection, respectively, with their relative magnitude defined by the parameter α_D. The function $\mathbf{O}_R$ just expresses the direction of the reflected ray $\mathbf{\Omega}_w$ through the direction of the incident one $\mathbf{\Omega}'_w$. This form of the reflection operator corresponds to the case where one takes into account the detailed structure of the wall exactly. In Sec. IV it will be shown that one can introduce a probabilistic approach for the description of small scale self-similar structures on the wall.

The mirror properties can be better described through an absorption tensor $\overleftrightarrow{\mathbf{A}}$ and a mode conversion tensor $\overleftrightarrow{\mathbf{C}}$,

$$\overleftrightarrow{\mathbf{M}}=\overleftrightarrow{\mathbf{C}}-\overleftrightarrow{\mathbf{A}}, \tag{33}$$

with

$$\overleftrightarrow{\mathbf{A}}=\begin{pmatrix} A^{(O)} & 0\\ 0 & A^{(X)}\end{pmatrix},\quad \overleftrightarrow{\mathbf{C}}=\begin{pmatrix} C^{OO} & C^{OX}\\ C^{XO} & C^{XX}\end{pmatrix}. \tag{34}$$

From energy conservation one can see that the following relations must hold:

$$C^{OO}=1-C^{XO},\quad C^{XX}=1-C^{OX}. \tag{35}$$

The wall absorption coefficients $A^{(M)}$ are usually described in terms of the wall reflection coefficient $\Gamma^{(M)}$ with the simple relation

$$A^{(M)}(\mathbf{\Omega}'_w)=1-\Gamma^{(M)}(\mathbf{\Omega}'_w). \tag{36}$$

So without any mode conversion the tensor for mirror reflection just becomes

$$\overleftrightarrow{\mathbf{M}}(\mathbf{\Omega}'_w)=\begin{pmatrix} \Gamma^{(O)}(\mathbf{\Omega}'_w) & 0\\ 0 & \Gamma^{(X)}(\mathbf{\Omega}'_w)\end{pmatrix}. \tag{37}$$

The normalization of the diffusive part follows from energy conservation during reflection and is given as

$$\int d\mathbf{\Omega}'_w[R_D^{OO}(\mathbf{\Omega}'_w,\mathbf{\Omega}_w)+R_D^{XO}(\mathbf{\Omega}'_w,\mathbf{\Omega}_w)]=1,\qquad \int d\mathbf{\Omega}'_w[R_D^{OX}(\mathbf{\Omega}'_w,\mathbf{\Omega}_w)+R_D^{XX}(\mathbf{\Omega}'_w,\mathbf{\Omega}_w)]=1. \tag{38}$$

For the calculation of the power loss from a plasma, one needs the intensity which is absorbed in the wall, $\mathbf{I}_{\rm out}(\mathbf{y}_w)$. It is denoted as outgoing intensity because it is leaving the

plasma. It can be calculated from the incident intensity $\mathbf{I}_{\mathrm{inc}}(\mathbf{y}_w)$ with the help of the absorption tensor $\overleftrightarrow{\mathbf{A}}$ through

$$\mathbf{I}_{\mathrm{out}}(\mathbf{y}_w)=\overleftrightarrow{\mathbf{A}}\mathbf{I}_{\mathrm{inc}}(\mathbf{y}_w). \tag{39}$$

The volume average of the power loss given by Eq. (10) can be expressed through this intensity with the help of the equation of the radiation transfer (2) and Gauss's theorem as given by

$$P=\frac{1}{V}\sum_{M=O,X}\int_V d^3V\, p^{(M)}(\mathbf{r}) \tag{40}$$

$$=\frac{1}{V}\sum_{M=O,X}\int_V d^3V\int_0^\infty d\omega\int_{4\pi} d^2\Omega \times \mathrm{div}[\hat{\mathbf{k}}I_\omega^{(M)}(\omega,\mathbf{r},\mathbf{\Omega})] \tag{41}$$

$$=\frac{1}{V}\sum_{M=O,X}\oint_S d^2S\int_0^\infty d\omega\int_{2\pi} d^2\Omega_w\, I_{\mathrm{out}}^{(M)}(\omega,\mathbf{r}_w,\mathbf{\Omega}_w). \tag{42}$$

It should be discussed here under what circumstances the four-dimensional Fredholm integral equation of the second kind, Eq. (18), can be reduced to lower dimensionality. For systems with toroidal symmetry, one has symmetry over one spatial coordinate which is the toroidal angle ζ. But of course, for the boundary problem of interest here, not only plasma properties have to be independent of ζ, but also wall structures. If this is the case, the dimensionality is reduced to three with the triple set of variables $(\Theta_w,\Phi_w,\vartheta_w)$. This cannot be further reduced in the case of a toroidal plasma.

The easiest situation one can find is for a cylindrical symmetry (infinite cylinder) with only mirror-like reflection at the first wall. Because of the fact that in this case the angles Θ_w and Φ_w are preserved during reflection and that all parts of the surface are identical, one can reduce the dimensionality to zero, leaving just a system of two algebraic equations,

$$\mathbf{I}_{\mathrm{inc}}(\mathbf{y}_w)=\overleftrightarrow{\mathbf{D}}(\mathbf{y}_w)\overleftrightarrow{\mathbf{M}}(\mathbf{y}_w)\mathbf{I}_{\mathrm{inc}}(\mathbf{y}_w)+\mathbf{I}_{\mathrm{gen}}(\mathbf{y}_w), \tag{43}$$

which can be easily solved. This, of course, is also true for an infinite slab geometry with the same reflection and surface properties. These are the only cases where the boundary problem can be solved analytically.

If one adds a diffusive part to the reflection tensor $\overleftrightarrow{\mathbf{R}}$ in the cylindrical case, one ends up with two dimensions, namely with the pair of variables (Θ_w,Φ_w), which in turn prohibits an analytical solution.

IV. SOLUTION OF THE BOUNDARY PROBLEM WITH FISH-SCALE-LIKE STRUCTURES ON THE FIRST WALL

The final goal here is to solve the boundary problem for an infinite cylinder with fish-scale structures in the z direction. Such a fish-scale-like structure is shown in Fig. 1.

The length l_F of the structure can be very small and should stay in the range of several wavelengths of the interesting part of the radiation. So this is in the range of millimeters to centimeters, which is to be compared to the overall size of the device in the range of a few meters.

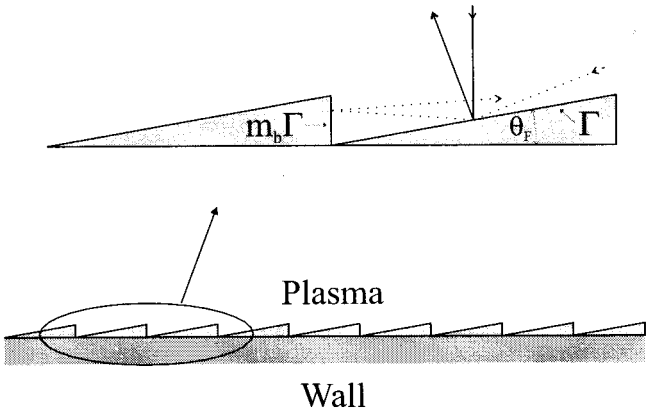

FIG. 1. Fish-scale structure with two ray examples.

As in the cylindrical case without fish-scale structures, the variable ϑ_w (poloidal angle) can be immediately removed from the Fredholm type integral equation. But now the wall structure is no longer independent of $\zeta_w\equiv z$. In principle, one can solve the problem in a general form using Eq. (32), but this demands a lot of computational effort because very fine resolution over the space variable is needed. However, a natural small parameter exists which allows us to simplify the problem with small-scale self-similar structures through introduction of a probabilistic approach. The huge difference in the scale of fish-scale structures l_F and the plasma size a helps to resolve this problem, because a small error in the fish-scale angle δl_F introduces a big enough error in the final position of the ray, i.e.,

$$\frac{\delta z}{l_F}\approx\frac{a\,\delta\Theta_F}{l_F}\gg 1. \tag{44}$$

This is always true for real surfaces with some irregularities.

This situation permits the use of probabilities to describe the different possibilities for the ray to hit the surface either on a fishscale surface (''good surface'') or on a perpendicular surface (''bad surface''). A ray might even hit these different parts of the surface two or three times before it finally returns to the plasma. These different parts of the surface are labeled good and bad because they give the desired directionality or the undesired, opposite one, respectively.

From pure geometrical considerations, one can derive the relations between incoming and outgoing angles during the reflection process for certain ranges of incoming angles, or the sequence in which good (g) and bad (b) surfaces are hit and the pertinent probability. All this is given in Table I. which was computed for fish-scale angles in the range $0<\Theta_F<\pi/8$. One can easily see from the results that fish-scale angles outside this range are of no practical interest.

The probabilities in Table I are specified as

TABLE I. Reflection on fish-scale structures.

Incoming			Surface	Probability	Outgoing
0	$<\Theta'<$	$\pi/2-\Theta_F$	g	1	Θ_1
$\pi/2-\Theta_F$	$\leqslant\Theta'<$	$\pi/2$	g	p_1	Θ_1
			gb	$1-p_1$	Θ_2
$\pi/2$	$\leqslant\Theta'<$	$\pi/2+\Theta_F$	g	$1-p_2-p_3$	Θ_1
			gb	p_2	Θ_2
			bgb	p_3	Θ_3
$\pi/2+\Theta_F$	$\leqslant\Theta'<$	$\pi-3\Theta_F$	g	$1-p_2-p_3$	Θ_1
			gb	p_2	Θ_2
			bg	p_3	Θ_4
$\pi-3\Theta_F$	$\leqslant\Theta'<$	$\pi-2\Theta_F$	g	$1-p_2-p_3$	Θ_1
			gb	p_1	Θ_2
			bg	p_3	Θ_4
			gbg	p_2-p_1	Θ_5
$\pi-2\Theta_F$	$\leqslant\Theta'<$	$\pi-\Theta_F$	bg	p_3	Θ_4
			gbg	$1-p_3$	Θ_5
$\pi-\Theta_F$	$\leqslant\Theta'<$	π	bg	1	Θ_4

$$p_1=\frac{\sin(\Theta'+2\Theta_F)}{\sin\Theta'},$$

$$p_2=-\tan\Theta_F\,\frac{\cos(\Theta'+2\Theta_F)}{\sin\Theta'}, \tag{45}$$

$$p_3=-\tan\Theta_F\cot\Theta',$$

whereas the outgoing angles are given as

$$\begin{aligned}
\Theta_1(\Theta',\Theta_F)&=\pi-\Theta'-2\Theta_F,\\
\Theta_2(\Theta',\Theta_F)&=\Theta'+2\Theta_F,\\
\Theta_3(\Theta',\Theta_F)&=\pi-\Theta'+2\Theta_F,\\
\Theta_4(\Theta',\Theta_F)&=\Theta'-2\Theta_F,\\
\Theta_5(\Theta',\Theta_F)&=2\pi-\Theta'-4\Theta_F.
\end{aligned} \tag{46}$$

It must be noted here, that all these angles are measured from a smooth surface without fish-scale structures. So, any dependence on the actual position at the first wall is avoided. Here one does not consider any diffusive contribution to the reflection process, therefore the reflection tensor used in Eq. (29) can be written as

$$\overleftrightarrow{\mathbf{R}}(\mathbf{\Omega}_w,\mathbf{\Omega}'_w)=\sum_i\, p_i(\Theta')\,\delta(\mathbf{\Omega}_w-\mathbf{O}_{Ri}(\mathbf{\Omega}'_w))\overleftrightarrow{\mathbf{M}}_i(\Theta'). \tag{47}$$

Here $p_i(\Theta')$ are the probabilities specified in Table I for each possible range of Θ'. The angular relation for the reflection $\mathbf{O}_{Ri}(\Omega'_w)$ is given as

$$\mathbf{O}_{Ri}(\mathbf{\Omega}'_w)=\begin{pmatrix}\Theta_{wi}\\ \Phi'_w\end{pmatrix}. \tag{48}$$

Here $\Theta'=\Theta'(\Theta'_w,\Phi'_w)$ and $\Theta_{wi}=\Theta_i^w(\Theta'_w,\Phi'_w)$ are defined through the relations

$$\begin{aligned}
\tan\Theta'&=\tan\Theta'_w\cdot\cos\Phi'_w,\\
\tan\Theta_i^w&=\tan\Theta_i(\Theta',\Theta_F)/\cos\Phi'_w,
\end{aligned} \tag{49}$$

where $\Theta_i(\Theta',\Theta_F)$ are the outgoing angles given in Eq. (46). The mirror reflection tensor used in Eq. (47) is given as

$$\overleftrightarrow{\mathbf{M}}_i(\Theta')=\begin{pmatrix}\Gamma_i^{(O)}(\Theta') & 0\\ 0 & \Gamma_i^{(X)}(\Theta')\end{pmatrix}, \tag{50}$$

where

$$\Gamma_i^{(M)}(\Theta')=(m_b)^{(\#b_i)}(\Gamma^{(M)})^{(\#b_i+\#g_i)}. \tag{51}$$

Here $\#b_i$ and $\#g_i$ are the respective numbers of reflections on a bad or good surface, and m_b is the ratio between the reflection coefficients $\Gamma^{(M)}$ on bad and on good surfaces.

Note that in the general case of wall absorption there is some mode conversion during the reflection process. However, for walls with good reflectivity the amount of energy transfered to the converted modes is proportional to the square of the absorption coefficient and should be neglected as small compared to the one absorbed by the wall. On the other hand, even for a plain wall the reflection coefficients $\Gamma^{(M)}$ are functions of both angles of incidence Θ'_w and Φ'_w. For simplicity this dependence is neglected, and the dependence on Θ' caused by different reflections scenarios as given by Eq. (51) is kept to show the influence of the fish-scale structure.

With the angular relation for the propagation in cylindrical symmetry

$$\mathbf{O}_P(\mathbf{\Omega}''_w)\equiv\begin{pmatrix}\pi-\Theta''_w\\ \Phi''_w\end{pmatrix}=\begin{pmatrix}\Theta_w\\ \Phi_w\end{pmatrix}, \tag{52}$$

one can write the appropriate transformation operator as

$$\begin{aligned}
\hat{\mathbf{K}}\cdot\mathbf{I}_{\rm inc}=&\int_0^{\pi}d\Theta'_w\int_{-\pi/2}^{\pi/2}d\Phi'_w\,\frac{\sin^2\Theta'_w\cos\Phi'_w}{\sin^2\Theta_w\cos\Phi_w}\\
&\times\overleftrightarrow{\mathbf{D}}(\Theta_w,\Phi_w)\sum_i\, p_i(\Theta'(\Theta'_w,\Phi'_w))\\
&\times\delta[\pi-\Theta_w-\Theta_{wi}(\Theta'_w,\Phi'_w)]\,\delta(\Phi_w-\Phi'_w)\\
&\times\overleftrightarrow{\mathbf{M}}_i(\Theta'(\Theta'_w,\Phi'_w))\mathbf{I}_{\rm inc}(\Theta'_w,\Phi'_w).
\end{aligned} \tag{53}$$

or after integration over Φ'_w one gets the final expression for the transformation operator

$$\begin{aligned}
\hat{\mathbf{K}}\cdot\mathbf{I}_{\rm inc}=&\overleftrightarrow{\mathbf{D}}(\Theta_w,\Phi_w)\int_0^{\pi}d\Theta'_w\,\frac{\sin^2\Theta'_w}{\sin^2\Theta_w}\\
&\times\sum_i\, p_i(\Theta'(\Theta'_w,\Phi_w))\\
&\times\delta[\pi-\Theta_w-\Theta_i^w(\Theta'_w,\Phi_w)]\overleftrightarrow{\mathbf{M}}_i(\Theta'(\Theta'_w,\Phi_w))\\
&\times\mathbf{I}_{\rm inc}(\Theta'_w,\Phi_w),
\end{aligned} \tag{54}$$

which gives the final formulation of the Fredholm problem, Eq. (18). It is evaluated numerically using the direct iteration method (construction of a Fredholm series). The procedure is obviously converging as long as there is any absorption

mechanism for the radiation, either absorption in the plasma or absorption at the wall. For all the necessary integrations, highly adaptive quadrature routines were developed which can handle integrations for the X- and O-mode in a very efficient, parallel way.

V. REFERENCE PARAMETER SET

For all the calculations, parabolic profiles are used for the radial dependence of temperature and density. The magnetic field strength can be varied along the radius according to the diamagnetic effect of the plasma pressure. The profiles are given as

$$T_e(r)=\langle T_e\rangle(\alpha_T+1)\,\frac{1+(q_T-1)[1-(r/a)^2]^{\alpha_T}}{\alpha_T+q_T}, \tag{55}$$

$$n_e(r)=\langle n_e\rangle(\alpha_n+1)\,\frac{1+(q_n-1)[1-(r/a)^2]^{\alpha_n}}{\alpha_n+q_n}, \tag{56}$$

$$B_z(r)=B_0\sqrt{1-f(r)\langle\beta\rangle}, \tag{57}$$

with

$$f(r)=\frac{\{1+(q_n-1)[1-(r/a)^2]^{\alpha_n}\}\{1+(q_T-1)[1-(r/a)^2]^{\alpha_T}\}}{F(\alpha_n,\alpha_T,q_n,q_T)}, \tag{58}$$

and

$$F(\alpha_n,\alpha_T,q_n,q_T)=1+(q_n-1)/(\alpha_n+1)+(q_T-1)/(\alpha_T+1)+(q_n-1)(q_T-1)/(\alpha_n+\alpha_T+1). \tag{59}$$

Here $\langle T_e\rangle$ and $\langle n_e\rangle$ are the mean electron temperature and the mean electron density, respectively, and $\langle\beta\rangle$ is the averaged β value.

The parameters α_n and α_T define the steepness of the profiles, whereas the parameters q_n and q_T give the ratio of the maximum to the edge value of $n_e(r)$ and $T_e(r)$ respectively.

In the case of diminishing edge values these formulas are simplified to a very widely used form

$$T_e(r)=\langle T_e\rangle(\alpha_T+1)[1-(r/a)^2]^{\alpha_T}, \tag{60}$$

$$n_e(r)=\langle n_e\rangle(\alpha_n+1)[1-(r/a)^2]^{\alpha_n}, \tag{61}$$

$$B_z(r)=B_0\sqrt{1-f(r)\langle\beta\rangle}, \tag{62}$$

with

$$f(r)=(\alpha_n+\alpha_T+1)[1-(r/a)^2]^{\alpha_n+\alpha_T}. \tag{63}$$

If not otherwise specified, all the results are calculated with the basic parameter set given in Table II. The parameters Z_1, Z_2, M_1, M_2 are the charge and mass of ion sort one $\equiv$D and ion sort two $\equiv{}^3$He, respectively, and c_{21} is the concentration of the ion sort two relative to the ion sort one.

TABLE II. Basic parameter set.

Symbol	Dimension	Value	Symbol	Dimension	Value
a	[m]	3.0	$1/A$	[−]	0.0
B_0	[T]	10.0	C^{XO}	[−]	0.0
$\langle n_e\rangle$	[10^{20} m^{-3}]	1.0	C^{OX}	[−]	0.0
$\langle T_e\rangle$	[keV]	40.0	Θ_F	[deg]	10.0
α_n	[−]	1.0	m_b	[−]	0.0
α_T	[−]	1.0	Z_1	[−]	1.0
q_n	[−]	100.	Z_2	[−]	2.0
q_T	[−]	100.	M_1	[−]	2.0
Γ^X	[−]	0.95	M_2	[−]	3.0
Γ^0	[−]	0.95	c_{21}	[−]	0.0

VI. DISCUSSION OF RESULTS

The results of a self-consistent modeling of the radiation intensity distribution, and the radial profiles of power loss and toroidal current are presented in the following figures.

Figure 2 shows both the frequency dependence of cyclotron power loss $dP/d\omega$ [actually the outgoing intensity already integrated over $\mathbf{\Omega}_w$ in Eq. (40)] and the passively driven current $dJ_t/d\omega$.

The current is generated mainly in a narrow frequency band around the so-called ''cutoff'' frequency.[9] The maximum of the power loss comes from somewhat higher $\bar{\omega}$ values in the range around $\bar{\omega}=10$. The range of frequencies can be divided into three regions: (i) The optically thick region at

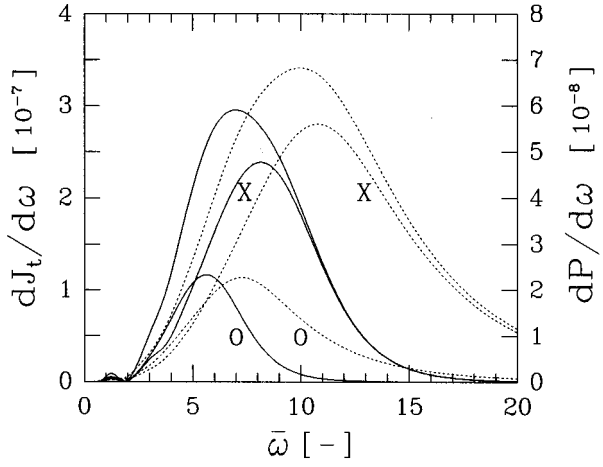

FIG. 2. Power loss per unit frequency, $dP/d\omega$ (dotted line), and plasma current per unit frequency, $dJ_t/d\omega$ (solid line), vs dimensionless frequency. The contribution from the two modes of propagation—X,O—is also shown.

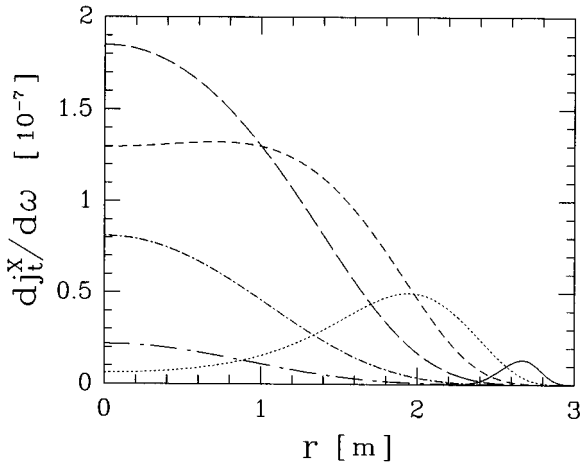

FIG. 3. Contribution of various frequencies to the toroidal current density vs radius for the X mode. Here $\overline{\omega}=2.5$ (solid line); $\overline{\omega}=5.0$ (dotted line); $\overline{\omega}=7.5$ (short-dashed line); $\overline{\omega}=10.0$ (long-dashed line); $\overline{\omega}=12.5$ (short-dash–dotted line); and $\overline{\omega}=15.0$ (long-dash–dotted line).

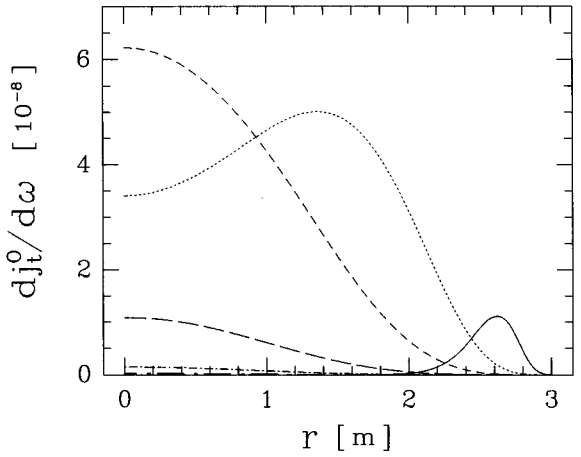

FIG. 4. Contribution of various frequencies to the toroidal current density vs radius for the O mode. Here $\overline{\omega}=2.5$ (solid line); $\overline{\omega}=5.0$ (dotted line); $\overline{\omega}=7.5$ (short-dashed line); $\overline{\omega}=10.0$ (long-dashed line); $\overline{\omega}=12.5$ (short-dash–dotted line); and $\overline{\omega}=15.0$ (long-dash–dotted line).

low frequencies, which does not give a significant contribution to the power loss and the current. But this region strongly determines the local power balance, keeping the distribution function close to a Maxwellian one. (ii) The intermediate region (thick–thin interface), where reflected rays easily penetrate the plasma and have some probability for reabsorption. Therefore, here the asymmetry generated by the fish-scale structure at the wall is transported into the plasma. This in turn generates the small δf responsible for the passively driven current. The region contributing to the current has a somewhat lower boundary. A reason for this is that the absorption coefficient dependence on the wave pitch angle becomes very peaked around $\Theta=\pi/2$ for higher frequencies. This results in poor reabsorption of the asymmetric part of the radiation created by the fish-scale structures. So the contribution to the current becomes smaller, whereas the contribution to the power loss becomes bigger. (iii) The optically thin region, contributing mainly to the losses but not the current, because with the low amount of reabsorption in this frequency region almost no asymmetry is generated in the plasma.

Here, and also in the following figures, the dominant contribution of the X mode to the current and to the power loss, as compared to the O mode, can be seen.

Figures 3 and 4 show the radial profile of the quantity $dj_t/d\omega$ which represents the contribution of different frequencies to the passive current density. One can easily see the difference between the optically thick region, the intermediate region, and the optically thin region. So, for low frequencies (thick) asymmetries are not transported far into the plasma and there is only a contribution to the current at the edge. Intermediate frequencies give a contribution in the center, whereas high frequencies (thin) are not reabsorbed very well. The two modes of propagation differ a little bit, reflecting more or less the lower values of the absorption coefficient and of the current drive efficiency for the O mode.

Figures 5 and 6 show the radial profiles of the net power loss $p(r)$, Eq. (10), and of the toroidal current density $j_t(r)$, Eq. (13). The main contribution to both quantities comes from the high temperature region in the plasma core. The loss profile shows the well-known effect of a net power deposition in the low temperature region at the edge which leads to a nonlocal energy transport in the plasma.

It is a remarkable fact, that the profile of the current presented for a case without toroidicity in Fig. 6 is very similar to the relevant curve given in Ref. 5. The current density profile in this reference was plotted just as a result of simple scaling laws. However, the absolute value of the current is too optimistic in Ref. 5. For a reactor parameter set corresponding to the density-weighted temperature of 37.7 keV listed in Table II of Ref. 5, a total cyclotron current of 8.87 MA is reported, while the calculation performed for the same set with the technique used in this paper gives a current

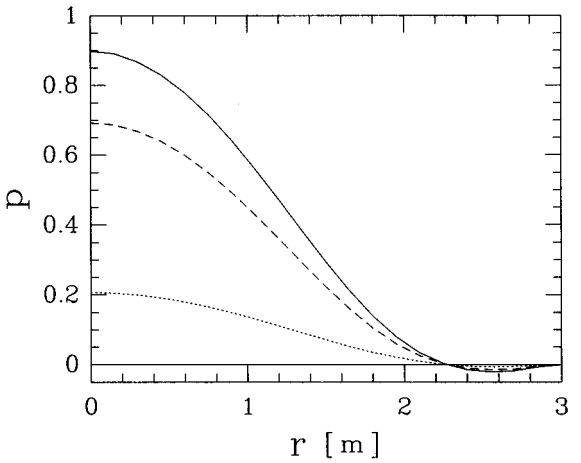

FIG. 5. Cyclotron power loss vs radius for the X mode (dashed line), for the O mode (dotted line), and the sum of both modes (solid line).

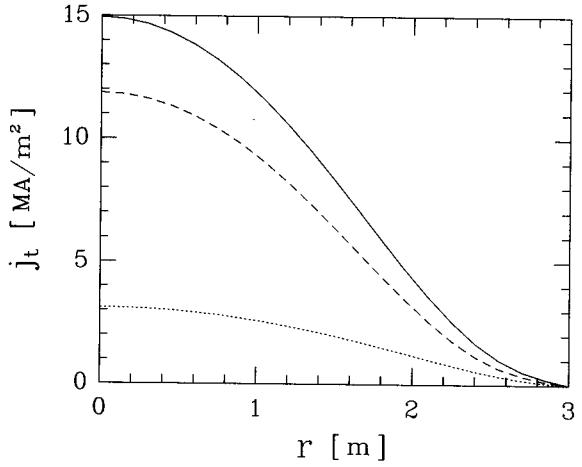

FIG. 6. Toroidal current density vs radius for the X mode (dashed line), for the O mode (dotted line), and the sum of both modes (solid line).

of 3.1 MA. One should note, that in the model used in the present paper the background electron response contributes significantly to the current, while this term is completely absent in the analysis in Ref. 5. The calculation without this response, in which Fisch's asymptotical formula was used gives even a smaller value of the total current being 1.7 MA.

Figure 7 shows the influence of toroidicity on the current density profile. The parameter which is actually varied is the inverse aspect ratio $\epsilon_t = 1/A = a/R_0$. It shows the strong influence of toroidicity even in central regions with low ϵ_t values, producing a very peaked profile. This decrease of the passive current drive efficiency is produced by the increase of the momentum loss cone size (phase space domain of trapped electrons). This size is proportional to $\sqrt{\epsilon_t}$. In addition to this, the positive contribution of the integral part is also strongly reduced.[9]

The influence of toroidicity on the total current J_t is demonstrated in Table III for different scenarios. This influence is roughly the same for different input parameters, e.g., plasma size or profile parameters, as long as the exact formula (EX) for the current drive efficiency is used. As discussed above, the influence of toroidicity is much smaller, when the asymptotical formula (FI) for the current drive efficiency[5] is used.

TABLE III. Influence of toroidicity on the total current.

	$\epsilon_t = 1/A$		
	0.0	0.1	0.2
a [m]		J_t [MA]	
2.0	11.7	7.2	5.5
3.0	22.0	13.6	10.4
4.0	34.4	21.3	16.4
$\alpha_n = \alpha_T$		J_t [MA]	
1.0	22.0	13.6	10.4
0.5	14.6	8.4	6.1
0.2	11.5	6.1	4.3
C_{mod}		J_t [MA]	
EX	22.0	13.6	10.4
FI	12.3	11.4	10.7

The influence of profile parameters on the current density is shown in Figs. 8 and 9. The influence of the density profile parameter α_n is less pronounced. A flatter density profile (lower values of α_n) with constant average density gives just a slight increase of the central current density, mainly because of the reduction of the influence of Coulomb collisions. The consequence of a change of the temperature profile parameter α_T is quite dramatic. A reduction of α_T to lower values, which represents a flatter profile at constant average temperature, completely changes the shape of the current density profile from steep to flat. So, the central temperature is much more important for passive current production than the average temperature. These results can also be seen in Table IV for the total current J_t. One can also see that the steepness of the temperature profile has a strong

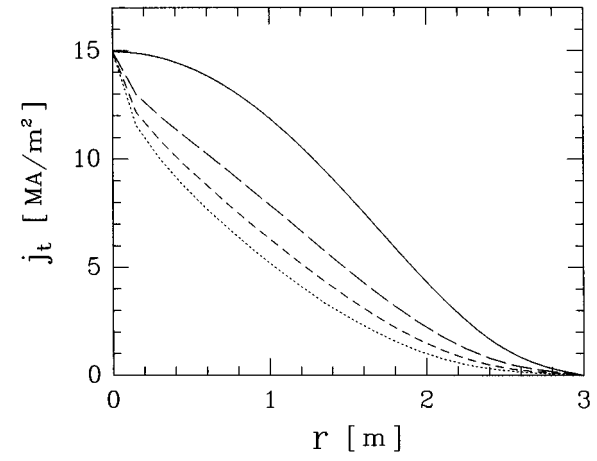

FIG. 7. Toroidal current density vs radius for various inverse aspect ratios $1/A = 0.0$ (solid line), $1/A = 0.1$ (long-dashed line), $1/A = 0.2$ (short-dashed line), and $1/A = 0.3$ (dotted line).

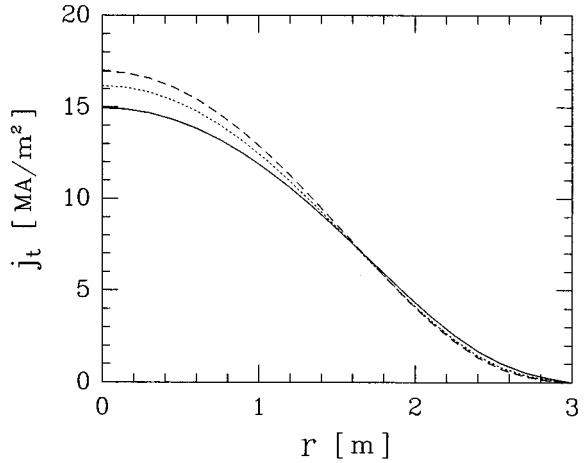

FIG. 8. Toroidal current density vs radius for various values of the density profile parameter $\alpha_n = 1.0$ (solid line), $\alpha_n = 0.5$ (dotted line), and $\alpha_n = 0.2$ (dashed line).

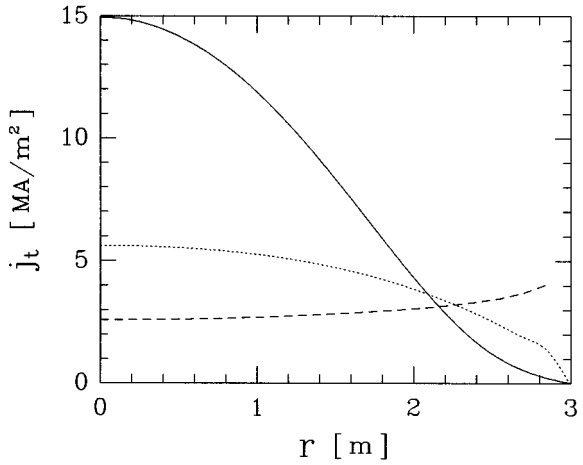

FIG. 9. Toroidal current density vs radius for various values of the temperature profile parameter $\alpha_T=1.0$ (solid line), $\alpha_T=0.5$ (dotted line), and $\alpha_T=0.2$ (dashed line).

influence on the power loss per unit volume P, whereas the density profile again is just of minor importance.

As one can see in Table V for $\epsilon_t=0$, the background electron response (integral part of the Coulomb collision operator—INT) contributes significantly to the total current, whereas the radiation collision force (radiation collision operator—RCO) always has a negative influence. The symbols FI and EX in Table V indicate that calculations are done with current drive efficiencies from Ref. 4 or with the exact ones derived within the framework of this paper. As shown before, the gain from the integral part, however, is quickly reduced with an increase of toroidicity.

Approximate scaling laws, both for the power loss per unit volume and the total current, are given in Table VI. The dependence on $\langle n_e \rangle$ is quite different, reflecting the increase of current with a decrease in density. This is an obvious consequence of the Coulomb resistivity decrease with decreasing density. The scaling with $\langle T_e \rangle$ is quite strong, making the electron temperature one of the key parameters for passive cyclotron current drive. The dependence on B_0 is roughly the same for both quantities (current and power) and also quite strong.

When the ^{3}He concentration is changed from $c_{21}=0$ to $c_{21}=1$ (same density of D and ^{3}He under the assumption of constant electron density) the total current is reduced from 22.0 to 15.8 MA. Values in between can be roughly calculated using the factor $1-0.28c_{21}$.

TABLE IV. Dependence of total current J_t and power loss per unit volume P on profile parameters.

	J_t [MA]			P [MW/m^3]		
α_T		α_n			α_n	
	0.2	0.5	1.0	0.2	0.5	1.0
1.0	22.4	22.1	22.0	0.70	0.75	0.80
0.5	14.3	14.6	15.4	0.50	0.52	0.55
0.2	11.5	12.2	13.8	0.41	0.42	0.42

TABLE V. Influence of the calculation procedures on the total current J_t.

C_{mod}	INT	RCO	J_t [MA]
EX	1	1	22.0
EX	1	0	24.4
EX	0	1	14.1
EX	0	0	15.7
FI			12.3

Figure 10 presents the toroidal current density $\tilde{j}_t=d^2j_t/(d\Theta d\omega)$ generated per unit frequency and unit wave pitch angle in the plasma center as a function of the wave pitch angle Θ. This quantity has an extremum for angles $\Theta=\pi/2\pm\pi/6$ and has a small asymmetry because of the smallness of the asymmetry of the intensity in angular regions close to $\Theta=\pi/2$ where the absorption is strong enough. The kernel of the net current production $-\tilde{j}_t(r,\Theta)-\tilde{j}_t(r,\pi-\Theta)$ is shown in Fig. 11. It has a maximum for angles a little bit smaller than $\pi/4$. This corresponds very well with the result in Ref. 4.

Figure 12 shows the power loss per unit frequency and unit wave pitch-angle $d^2P/(d\Theta d\omega)$ for various fish-scale angles and m_b ratios. This shows a dramatic increase of losses for angles $\Theta_w>\pi/2$, in the case of low reflectivity at the bad surface and for fish-scale angles in the range from 5° to 15° or even more. So intensity is shifted to larger angles and then is effectively lost to the wall. This happens mainly at the bad surface, because rays with large angles Θ_w have a higher probability to hit the bad surface compared to those with smaller angles.

Figure 13 shows the total current as a function of the fish-scale angle with parametric dependence on m_b for the case of zero toroidicity. A remarkable fact is that the behavior of the current as a function of Θ_F and m_b is quite similar both for the cases of zero and finite toroidicity, despite the fact that the magnitude of the current is quite different (see Table III).

The current increases rapidly for fish-scale angles up to $\Theta_F\approx 10°$ and quickly saturates for higher angles because too much radiation is lost to the wall. The best results can be obtained for $m_b=0$ (no reflection from the bad wall). Results for $m_b=1$ (same reflectivity at the bad surface as at the good one) are roughly a factor of 3 lower.

Figure 14 shows the increase of the power loss with increasing values of Θ_F and decreasing values of m_b, which is a quite understandable behavior. The global efficiency $J_t/\Delta p_{\mathrm{out}}$, where Δp_{out} is the difference in the power loss compared to the case without any fish-scale structure, but otherwise calculated under same conditions, is given in Fig. 15. It has a distinct maximum at lower fish-scale angles

TABLE VI. Approximate scaling relations.

	P	J_t
a	−0.5	1.5
$\langle n_e \rangle$	0.5	−0.2
$\langle T_e \rangle$	2.7	3.5
B_0	2.5	2.3

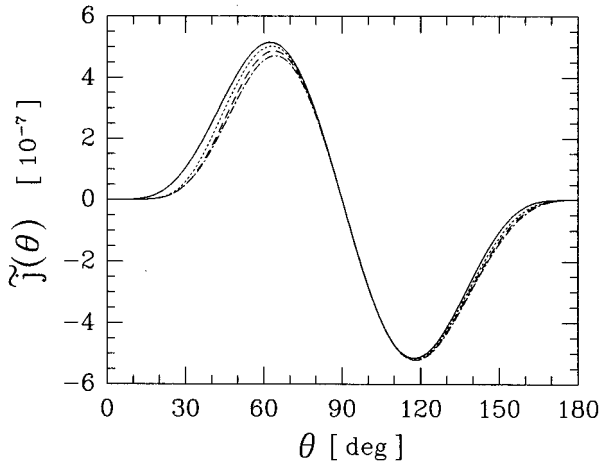

FIG. 10. Toroidal current density per unit frequency and wave pitch angle for the extraordinary mode as a function of Θ in the plasma center ($r=0$ m). Here $\overline{\omega}=7.5$; $m_b=0.0$; the fish-scale angle $\Theta_F=0°$ (solid line); $\Theta_F=5°$ (dotted line); $\Theta_F=10°$ (dashed line); and $\Theta_F=15°$ (dash–dotted line).

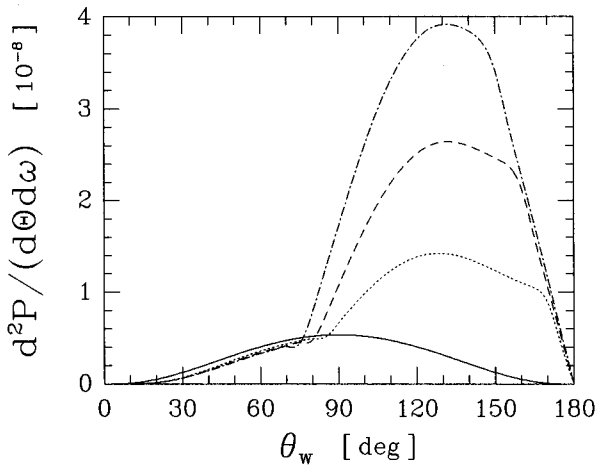

FIG. 12. Power loss per unit frequency and per unit wave pitch angle for the extraordinary mode as a function of Θ_w. Here $\overline{\omega}=7.5$; $m_b=0.0$; the fish-scale angle $\Theta_F=0°$ (solid line); $\Theta_F=5°$ (dotted line); $\Theta_F=10°$ (dashed line): and $\Theta_F=15°$ (dash–dotted line).

around $\Theta_F=5°$ and is much higher for $m_b=1$. However, it is hard to achieve at the same time high current (good at $\Theta_F=10°$, $m_b=0$) and high efficiency (good for $\Theta_F=5°$, $m_b=1$). So, in this respect a compromise always has to be found, depending on how much current is needed and how much additional losses can be accepted.

The value of the optimum fish-scale angle to achieve the highest efficiency differs from the estimate given in Ref. 1 which for $\Gamma=0.95$ gives $\Theta_F\approx 1.5°$.

Finally Figs. 16–17 give results as a function of the wall reflection coefficient Γ. It shows the decrease of the power loss with Γ approaching unity, which is not as strong for $m_b=0$ (relative reflectivity of bad surface), because there is always the remaining absorption at the bad surface. If $m_b=1$ the current does not change much with the variation of the

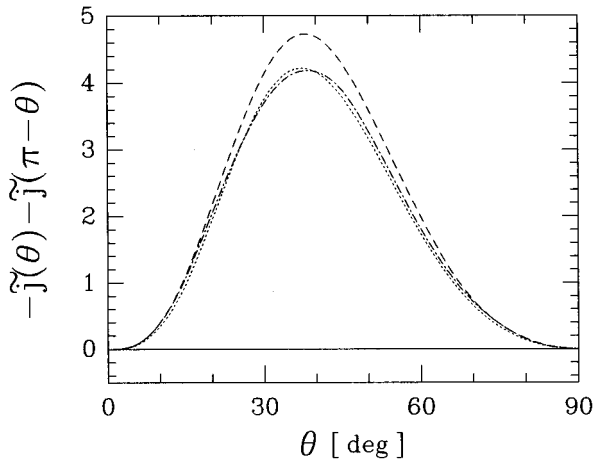

FIG. 11. Net toroidal current density per unit frequency and wave pitch angle for the extraordinary mode as a function of Θ in the plasma center ($r=0$ m). Here $\overline{\omega}=7.5$; $m_b=0.0$; the fish-scale angle $\Theta_F=0°$ (solid line); $\Theta_F=5°$ (dotted line); $\Theta_F=10°$ (dashed line); and $\Theta_F=15°$ (dash–dotted line).

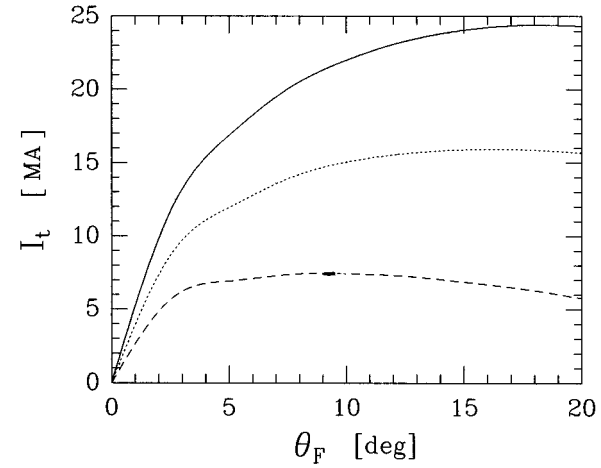

FIG. 13. Total plasma current vs fish-scale angle with the parameter $m_b=\Gamma_b/\Gamma=0.0$ (solid line), $m_b=0.5$ (dotted line), and $m_b=1.0$ (dashed line).

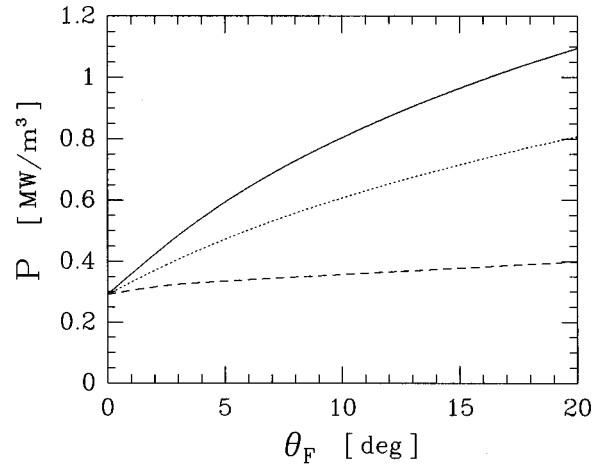

FIG. 14. Power loss per unit volume vs fish-scale angle with the parameter $m_b=0.0$ (solid line), $m_b=0.5$ (dotted line), and $m_b=1.0$ (dashed line).

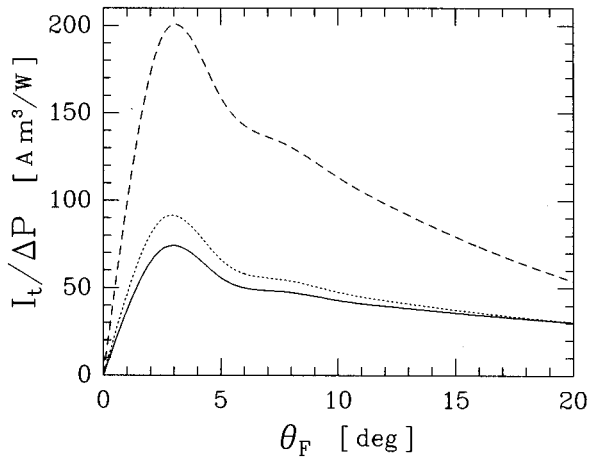

FIG. 15. Global current drive efficiency vs fish-scale angle with the parameter $m_b=0.0$ (solid line), $m_b=0.5$ (dotted line), and $m_b=1.0$ (dashed line).

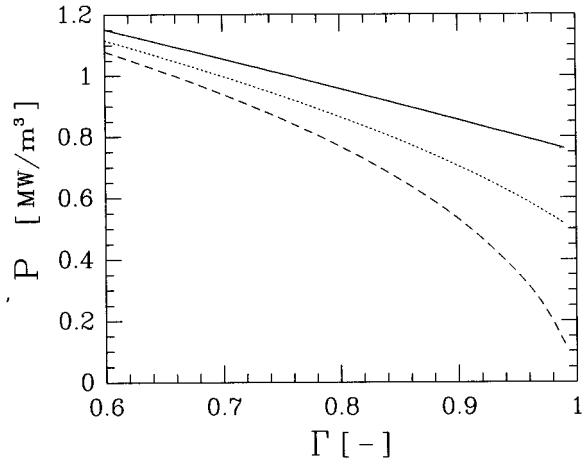

FIG. 17. Power loss per unit volume vs wall reflectivity Γ for a fish-scale angle of $\Theta_F=10°$ and the parameter $m_b=0.0$ (solid line), $m_b=0.5$ (dotted line), and $m_b=1.0$ (dashed line).

wall reflection coefficient, but increases for lower values of m_b. So again from the point of view of current generation it is better to operate at as high as possible wall reflection coefficients with very low values of the parameter m_b.

VII. CONCLUSION

From the results obtained, a reactor based on this method or at least partly sustained by this method should operate at high temperatures, high magnetic field strength and low density. In addition to this, high aspect ratio devices seem to be more suited to the use of this method if it is the only source of current drive.

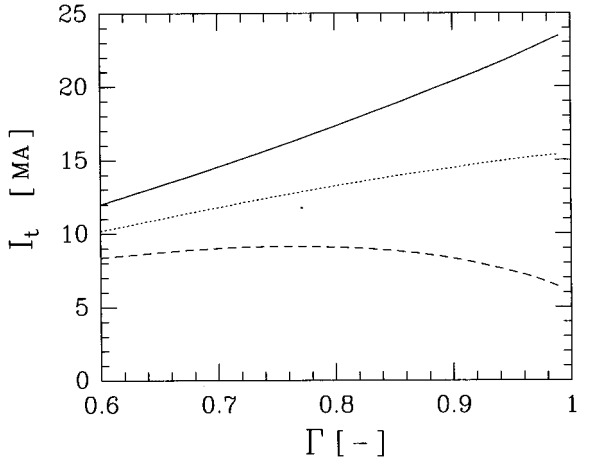

FIG. 16. Total plasma current vs wall reflectivity Γ for a fish-scale angle of $\Theta_F=10°$ and the parameter $m_b=0.0$ (solid line), $m_b=0.5$ (dotted line), and $m_b=1.0$ (dashed line).

Overall, it seems to be a very interesting current drive method suitable for either D–T or D–^{3}He high-temperature plasmas. One of the most interesting results is the fact that the current density profile is peaked in the center. So, this method could, in principle, act as a seed current for the bootstrap current and could also provide a large portion of the total current itself.

An open question is still: how much the full account of the toroidal geometry in the radiation transport process and in the interaction with the first wall would change the results. Another interesting question would be: how big must the fraction of the first wall covered with fish scales be for optimum performance. All of these is part of our continued research in this field.

ACKNOWLEDGMENTS

The authors would like to thank Professor K. N. Stepanov for valuable discussions.

This work was supported by the Austrian Academy of Sciences, the International Atomic Energy Agency, and the Styrian Government. One of the authors, S.V.K., acknowledges the financial support from the Technische Universität Graz and the hospitality at the Institut für Theoretische Physik during his scientific visit to Graz.

[1] J. Dawson and P. K. Kaw, Phys. Rev. Lett. **48**, 1730 (1982).
[2] R. Klima and A. Longinov, Sov. J. Plasma Phys. **5**, 277 (1979).
[3] N. Fisch, Phys. Rev. Lett. **41**, 873 (1978).
[4] I. Fidone, G. Granata, and J. Johner, Phys. Fluids **31**, 2300 (1988).
[5] J. Johner and I. Fidone, Nucl. Fusion **29**, 449 (1989).
[6] G. Giruzzi and I. Fidone, Nucl. Fusion **29**, 2235 (1989).
[7] I. Fidone, Phys. Fluids B **5**, 3825 (1993).
[8] W. Kernbichler and S. Kasilov, Trans. Fusion Technol. **27**, 423 (1995).
[9] S. Kasilov and W. Kernbichler, Phys. Plasmas **3**, 4115 (1996).
[10] M. Bornatici, O. De Barbieri, R. Cano, and F. Engelmann, Nucl. Fusion **23**, 1153 (1983).
[11] S. Tamor, Nucl. Technol./Fusion **3**, 293 (1983).